HOSTED BY
ELSEVIER
CrossMark
Available online at www.sciencedirect.com
ScienceDirect
Journal of Magnesium and Alloys 4 (2016) 62–67
www.elsevier.com/journals/journal-of-magnesium-and-alloys/2213-9567

Full Length Article

Atomic relaxation, stability and electronic properties of Mg_2Sn (100) surfaces from ab-initio calculations

Hui Ren [a], Wen-Cheng Hu [a], De-Jiang Li [b], Xiao-Qin Zeng [c], Xue Yang [a], Xiao-Shu Zeng [a], Xiang-Jie Yang [a], Bolong Huang [d], Yong Liu [a,*]

[a] *Key Laboratory of Near Net Forming of Jiangxi Province, Nanchang University, Nanchang 330031, China*
[b] *National Engineering Research Center of Light Alloys Net Forming, Shanghai Jiao Tong University, Shanghai 200240, China*
[c] *State Key Laboratories of Metal Matrix Composite, Shanghai Jiao Tong University, Shanghai 200240, China*
[d] *Department of Physics and Materials Science, City University of Hong Kong, Kowloon, Hong Kong*

Received 13 January 2016; accepted 2 February 2016

Available online 2 March 2016

Abstract

Mg_2Sn (100) surfaces were investigated using ab-initio method based on density functional theory in order to explore the surface properties. It is found that both the eleven-layers for Mg-termination surfaces and the nine-layers for Sn-termination surfaces are all converged very well. The effects of relaxation mainly occurred within the three outermost atomic layers for both Mg and Sn terminations during the surface relaxation. Mg-termination surfaces are more stable than Sn-termination surfaces according to the analysis of surface energy. The density of states reveals the metallic property of both Mg-termination and Sn-termination surfaces. Covalent bonding exists in Mg_2Sn (100) surfaces according to the analysis of partial density of states.

Keywords: Magnesium alloy; Ab-initio calculation; Surface energy; Surface stability; Electronic properties

1. Introduction

As the lightest metallic structure material, magnesium (Mg) and its alloys are increasingly used in many engineering areas including portable microelectronics, telecommunication, aerospace and automobile industries due to their low density, high specific strength, high specific stiffness and good machinability [1,2]. Among various Mg alloys, the Mg-Sn binary system is a typical precipitation hardening system. It is a candidate for high strength wrought Mg alloys due to its high strength, excellent corrosion resistance, high temperature superplastic deformation and extrusion capability at moderate temperature. In addition, the Mg_2Sn phase has a melting temperature of about 1043K, which impedes dislocation slipping at high temperature and improves the mechanical properties at the elevated temperature [3–7]. Recently, the anti-fluorite Mg_2X (X = Si, Ge, Sn and Pb) compounds have attracted more and more attention because they possess remarkably thermoelectric (TE) properties. These narrow band gap semiconducting compounds exhibit many advantages for potential TE applications due to the abundance of constituents, low density, non-toxicity and environmental friendliness [8]. Moreover, such semiconducting compounds are always used as model systems in which to study band structures of semiconductors and to form variable semiconductors with a band gap adjustable with the range of 0–0.78 eV [9].

In recent decades, a large amount of studies have been performed on Mg_2X compounds [10–12], especially on Mg_2Sn phase. Kim et al. [13] found that the optimum mechanical properties combination was obtained at the 3–5wt.% Sn in Mg-xSn-5Al-1Zn alloys. The excess Sn would coarsen the Mg_2Sn phase. Wang et al. [14,15] reported that as-cast Mg-3Sn-1Zn and Mg-3Sn-3Al alloys both exhibit strong strain hardening ability and high elongation, which implies that the alloy possesses good formability. Sasaki et al. [4,16,17] found that 1 at.% Al improved the hardening response on Mg-2.2Sn-0.5Zn (at.%) alloy, and the addition of Zn can change the morphology and density of the Mg_2Sn phases as well as enhance the age-hardening response. Chen et al. [18] studied the effects of Zn on

* Corresponding author. Key Laboratory of Near Net Forming of Jiangxi Province, Nanchang University, Nanchang 330031, China. Tel.: +86 79183968992; fax: +86 79183968992.
E-mail address: liuyong@ncu.edu.cn (Y. Liu).

http://dx.doi.org/10.1016/j.jma.2016.02.002
2213-9567/

the microstructure and mechanical properties of Mg-3Sn-1Al alloys. They found that the grain size decreased gradually and the amount of Mg_2Sn particles increased markedly with increasing Zn content. Le-Quoc et al. [8] studied the thin films of thermoelectric compound Mg_2Sn deposited by co-sputtering assisted by multi-dipolar microwave plasma. It was found that stoichiometric Mg_2Sn thin films doped with about 1 at.% Ag exhibit a high power factor at room temperature. Liu et al. [19] reported the influences of the quantity of Mg_2Sn phase on the corrosion behavior of Mg-7Sn alloy, which showed that the corrosion mode and corrosion rate was associated with the quantity of Mg_2Sn phases and Sn concentration of the matrix. Urretavizcaya et al. [20] reported that the metastable hexagonal Mg_2Sn could be obtained by mechanical alloying. They found that the metastable hexagonal structure of Mg_2Sn was produced during the process of milling and the hexagonal structure transformed into the stable Mg_2Sn phase at 713 K. Furthermore, the first-principles calculation based on density functional theory (DFT) is applied to study the properties of intermetallic compounds [21–24]. Yu et al. [25] studied the high-pressure phase transitions of Mg_2Ge and Mg_2Sn from first-principles calculations and found that the high pressure behaviors of Mg_2Ge and Mg_2Sn are similar to Mg_2Si and the isostructural alkali-metal oxide Li_2O. Defect, phase stability, temperature dependent elastic coefficients, thermal stability, elastic properties and ideal strength of Mg_2X with anti-fluorite structure from first-principles study were reported [26–29]. Our group [30] has also investigated the structural, electronic and thermodynamic properties of the anti-fluorite type Mg_2Sn under pressure, which indicates that the anti-fluorite type Mg_2Sn compound is mechanically stable up to 5.0 GPa and the bulk modulus increases with increasing pressure. However, to the best of our knowledge, most of the researches are mainly focused on the bulk properties of Mg_2Sn phase at equilibrium state and under high pressure.

In addition to the bulk properties, the properties of Mg_2Sn surfaces are not only basic scientific concerns, but also important for engineering applications. For instance, the combination between the Mg_2Sn particles and the metallic matrix could be influenced by the crystalline structure and the electronic properties of the Mg_2Sn surfaces. From this perspective, it is fairly necessary to investigate properties of Mg_2Sn surfaces for the advanced material design of Mg alloys with high performance. In this paper, we investigated the properties of Mg_2Sn (100) surfaces based on DFT within the generalized gradient approximation (GGA), including surface relaxation, surface stability and electronic structures. The results can provide theoretical insights in understanding Mg_2Sn (100) surfaces in order to extend the engineering application of Mg alloys.

2. Computational details

2.1. Computational method

Cambridge Serial Total Energy Package (CASTEP), a first-principles method based on DFT was used in this work for all calculations [31,32]. The electron–ion interactions was described by the ultrasoft pseudopotential [33,34]. The generalized gradient approximation (GGA) in form of the Perdew, Burke and Ernzefhof (PBE) was used for electron exchange and correlation [35]. The Broyden–Fletcher–Goldfarb–Shannon (BFGS) method was adopted to relax the atomic coordinates during the optimization [36,37]. Pseudoatomic calculations were performed for Mg $2p^6 3s^2$ and Sn $5s^2 5p^2$. The cutoff energy of plane waves was set to 450 eV and the Brillouin zone was sampled with K-points of $8 \times 8 \times 8$ for bulk Mg_2Sn phase. For Mg_2Sn (100) surfaces calculation, the cutoff energy was selected as 380 eV and the Brillouin zone was sampled with a $6 \times 6 \times 1$ K-point mesh. All atoms in bulk Mg_2Sn and Mg_2Sn (100) surfaces were fully relaxed to during the optimization until the total energy change was less than 5×10^{-6} eV/atom and maximum ionic displacement was within 5×10^{-4} Å.

Table 1
The calculated lattice parameters (Å), elastic constants (GPa) and elastic modulus (GPa) in comparison with the experimental and other theoretical values.

	a	C_{11}	C_{12}	C_{44}	B	G	E	Ref.
Cal.	6.826	75.7	23.6	33.5	40.9	30.1	64.5	Present
	6.825	69.8	25.9	31.1	40.5	27.4	67.1	[38]
	6.694	–	–	–	44.7	–	–	[25]
	6.829	68.1	25.9	28.9	40.61	25.4	62.9	[30]
Exp.	6.76	82.4	20.8	36.6	41.3	34.2	80.3	[38]
	6.75	–	–	–	41.2	–	–	[39]

2.2. Mg_2Sn (100) surface models

In order to guarantee the reliability of our work, the properties of bulk Mg_2Sn were calculated before the surface optimization. The anti-fluorite Mg_2Sn phase with the space group symmetry Fm-3m (No. 225) was used for calculation. The calculated lattice parameters, elastic constants and elastic moduli are listed in Table 1. It is found that the calculated lattice parameters are in excellent agreement with previous reports and the elastic constants match well with other reports [38,39]. These results show that our work is highly reliable.

After the optimization of bulk Mg_2Sn, the Mg_2Sn (100) surfaces with Sn-termination and Mg-termination were investigated. Mg_2Sn (100) surfaces were established by cleaving surfaces from the optimized bulk Mg_2Sn (1×1) supercell. Each layer in Sn-termination and Mg-termination surfaces consists of only one species of Mg atom or Sn atom. The surfaces model is made up of a slab model and a vacuum region [40]. Sn-termination and Mg-termination slab models of Mg_2Sn (100) surfaces is shown in Fig. 1, respectively. Therefore, Mg-termination (1×1) slabs with 7, 11, 15 layers and Sn-termination (1×1) slabs with 5, 9, 13 layers were employed for surface relaxation. In order to avoid atomic interaction between layers, a vacuum region with the thickness of 15 Å is included in surface models after a series of vacuum region thickness tests. In the process of geometry optimization, all atoms in the surface models were fully relaxed.

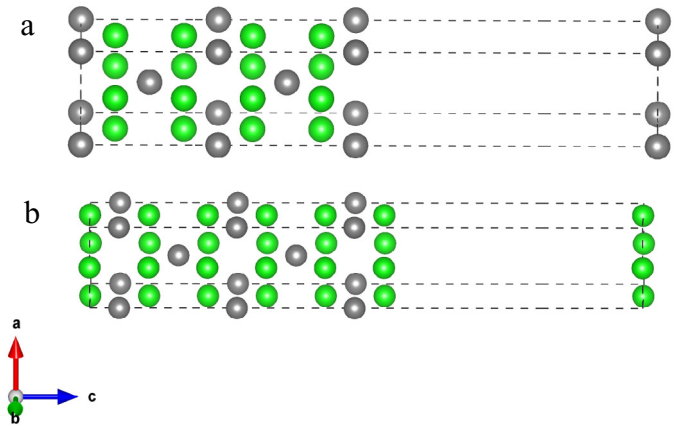

Fig. 1. Two types of slab models of the Mg_2Sn (100) surfaces along *c* axis. (a) Sn-termination, (b) Mg-termination. The gray ball and green ball denotes Sn atom and Mg atom, respectively.

3. Results and discussions

3.1. Atomic relaxations of Mg_2Sn (100) surfaces

There are 2 types of Mg_2Sn (100) surfaces: Mg-termination surfaces and Sn-termination surfaces. The results of slab thickness dependence of surface relaxation are listed in Table 2. The relative change of the layer distance is defined as Δd_{i-j}.

$$\Delta d_{i-j} = \left(d_{i-j} - d_0\right)/d_0 \times 100\% \quad (1)$$

Here, d_{i-j} denotes the layer distance between *i* layer and *j* layer, and d_0 refers to the specific inter-planar distance of unrelaxed surface models. $\Delta d_{i-j} < 0$represents that the layer distance deceases and $\Delta d_{i-j} > 0$ means an increase of the layer distance.

Surface reconstruction does not occur for Mg-termination and Sn-termination surfaces during the surface relaxation. From Table 2, it is found that the interlayer relaxations are all small. Meanwhile, the effects of relaxation are mainly localized within the three outermost atomic layers. The interlayer relaxations converged very well when the slab thickness (N) is larger than nine layers and eleven layers for Sn-termination surfaces and Mg-termination surfaces, respectively. The good convergence indicates that the slabs with enough layers behave a bulk-like interior. Thus, symmetric Sn-termination with 9 atomic layers and symmetric Mg-termination with 11 atomic layers were employed in the consecutive calculations. It is found that the outermost interlayer distance of Sn-termination with 9 atomic layers and that of Mg-termination with 11 atomic layers are equally increased by 1.641%. However, as for the second and third interlayers, the distance increments of Sn-termination are all larger than that of Mg-termination (1.814% > 1.705% for the second interlayer, 1.729% > 1.652% for the third interlayer, respectively), which implies that Mg-termination surfaces are likely more stable than Sn-termination surfaces.

Table 2
The relative change of the layer distance (Δd_{i-j}) as a function of different terminations and slab thickness (N).

Thickness(N)	Sn-termination			Mg-termination		
	5	9	13	7	11	15
Δd_{1-2}	0.193%	1.641%	1.634%	1.714%	1.641%	1.679%
Δd_{2-3}	1.866%	1.814%	1.669%	1.724%	1.705%	1.694%
Δd_{3-4}	2.004%	1.729%	1.790%	1.690%	1.652%	1.658%
Δd_{4-5}		1.742%	1.695%	1.688%	1.679%	1.675%
Δd_{5-6}		1.743%	1.699%		1.671%	1.663%
Δd_{6-7}			1.676%		1.666%	1.687%
Δd_{7-8}			1.678%			1.669%
Δd_{8-9}						1.671%

3.2. Surface stability of Mg_2Sn (100) surfaces

The stability of surfaces could be determined by surface energy. The lower the surface energy is, the more stable the surface is. For the purpose of obtaining the surface energies of both Sn-termination and Mg-termination surfaces, the chemical potentials of Mg atom and Sn atom are used for calculations. The surface energy of Mg_2Sn (100) surfaces, $\sigma_{Mg_2Sn(100)}$, is defined as follows [41–43]:

$$\sigma_{Mg_2Sn(100)} = \frac{1}{2A_{surface}}\left(E_{slab} - N_{Mg}\mu_{Mg}^{slab} - N_{Sn}\mu_{Sn}^{slab} + PV - TS\right) \quad (2)$$

where $A_{surface}$ refers to the surface area, E_{slab} denotes the total energy of a optimized Sn-termination or Mg-termination surface. N_{Mg} and N_{Sn} represents Mg atom number and Sn atom number in the surface model, respectively. μ_{Mg}^{slab} and μ_{Sn}^{slab} is the atomic chemical potentials of Mg and Sn in the slab, respectively. Under certain pressure *P* and temperature *T*, the *PV* and *TS* could be omitted in regard to other contributions [44]. All calculations in our work were performed at $P = 0$ GPa and $T = 0$ K, therefore the *PV* and *TS* terms were not taken into consideration.

In the fully relaxed surface structure, the Mg_2Sn (100) surfaces are in a state that is very similar to the bulk Mg_2Sn. Therefore, the chemical potential of bulk Mg_2Sn, $\mu_{Mg_2Sn}^{bulk}$, can be obtained by the following equation:

$$\mu_{Mg_2Sn}^{bulk} = 2\mu_{Mg}^{slab} + \mu_{Sn}^{slab} \quad (3)$$

The definition of chemical potential of bulk Mg_2Sn in thermodynamics, $\mu_{Mg_2Sn}^{bulk}$, is expressed by:

$$\mu_{Mg_2Sn}^{bulk} = 2\mu_{Mg}^{bulk} + \mu_{Sn}^{bulk} - \Delta H_f^0 \quad (4)$$

where μ_{Mg}^{bulk} and μ_{Sn}^{bulk} is the single atom energy in Mg bulk and Sn bulk, respectively. ΔH_f^0 refers to the formation heat of bulk Mg_2Sn at 0 K.

Integrated with equation (3), equation (2) is adapted as follows:

$$\sigma_{Mg_2Sn(100)} = \frac{1}{2A_{surface}}\left[E_{slab} - N_{Sn}\mu_{Mg_2Sn}^{bulk} + \left(2N_{Sn} - N_{Mg}\right)\mu_{Mg}^{slab}\right] \quad (5)$$

Integrating equation (3) with equation (4), the following equation can be acquired.

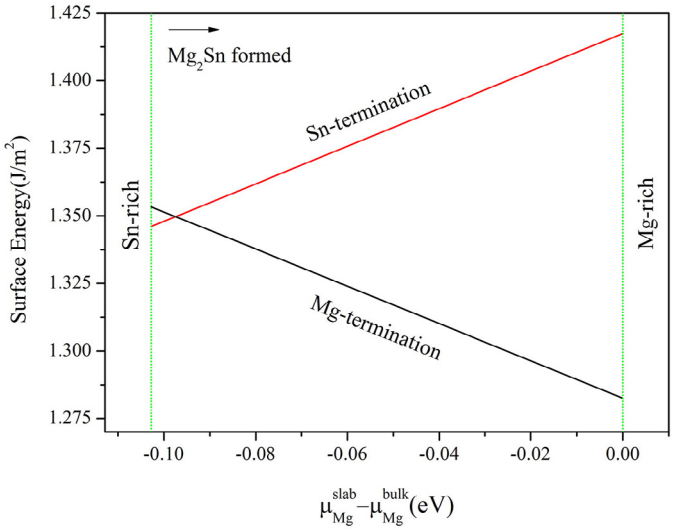

Fig. 2. Surface energy of Mg-termination and Sn-termination surfaces as a function of $\left(\mu_{Mg}^{slab}-\mu_{Mg}^{bulk}\right)$.

$$\mu_{Mg}^{slab}-\mu_{Mg}^{bulk}=\frac{1}{2}\left(\mu_{Sn}^{bulk}-\mu_{Sn}^{slab}+\Delta H_f^0\right) \tag{6}$$

Additionally, the chemical potentials of Mg and Sn atoms in the slab should be smaller than those in their bulk substance, respectively. This is because the higher chemical potentials of Mg and Sn atoms will result in the instability of the slabs. Therefore, the relationship between μ^{slab} and μ^{bulk} is $\mu_{Mg}^{slab}\le\mu_{Mg}^{bulk}$ and $\mu_{Sn}^{slab}\le\mu_{Sn}^{bulk}$ for Mg and Sn, respectively.

On the basis of equation (5), the following equation can be derived:

$$\frac{1}{2}\Delta H_f^0\le\mu_{Mg}^{slab}-\mu_{Mg}^{bulk}\le 0 \tag{7}$$

The calculated ΔH_f^0 is −0.2056 eV/atom, which is in excellent agreement with previous reports with the range from −0.213 to −0.278 eV/atom [45–47].

Based on equation (5), the surface energies of Mg-termination and Sn-termination surfaces were obtained. The results are shown in Fig. 2. It can be seen from Fig. 2, in initial small part of Sn-rich area, the surface energy of Mg-termination surfaces is slightly larger than that of Sn-termination surfaces, which indicates that Sn-termination surfaces may be slightly more stable than Mg-termination surfaces. However, it is obviously found that the surface energy of Mg-termination surfaces is much smaller than that of Sn-termination surfaces in nearly the whole area, which demonstrates that Mg-termination surfaces are much more stable than Sn-termination surfaces in nearly the whole area. This result accords with our above conclusion in Sec. 3.1. Moreover, the surface energy of Mg-termination surfaces presents a declining tendency with the increasing chemical potentials $\left(\mu_{Mg}^{slab}-\mu_{Mg}^{bulk}\right)$, which implies that Mg-termination surfaces continuously become more and more stable. To the best of our knowledge, however, there is no experimental data to compare with our results obtained by first-principles calculation.

3.3. Electronic properties

In order to further understand the properties of Mg_2Sn (100) surfaces, band structure and density of states (DOS) were also investigated from first-principles calculation. The band structures of Mg-termination and Sn-termination surfaces are shown in Fig. 3. It is found that there are no band gaps in band structures of Mg-termination and Sn-termination surfaces, which implies that the two termination surfaces are all metallic characterization. Meanwhile, it can be seen that the distribution range of Mg-termination surfaces is narrower than that of Sn-termination surfaces.

The total DOS for Mg-termination and Sn-termination surfaces are shown in Fig. 4. In general, the shape of total DOS for the two terminations are similar. To be careful, it can be found that the value of total DOS at Fermi level of Mg-termination surfaces is larger than that of Sn-termination surfaces. Moreover, as compared with Sn-termination surfaces, the energy area above Fermi level in total DOS of Mg-termination surfaces shifts to the lower energy, which indicates that Mg-termination surfaces possess a higher structural stability.

Detailed features of total DOS can be displayed by partial density of states (PDOS). The layer-atom PDOS of Mg-termination surfaces is shown in Fig. 5. It can be seen that the low energy area below Fermi level is mainly composed of Sn atoms, while the Mg atoms contribute to the high energy area above Fermi level. Moreover, the *p* states of the first Mg layer are different from those of the second and third Mg layers. The *p* states of the first Sn layer is distinct from those of the second and third Sn layers. It may be attributed to the stronger

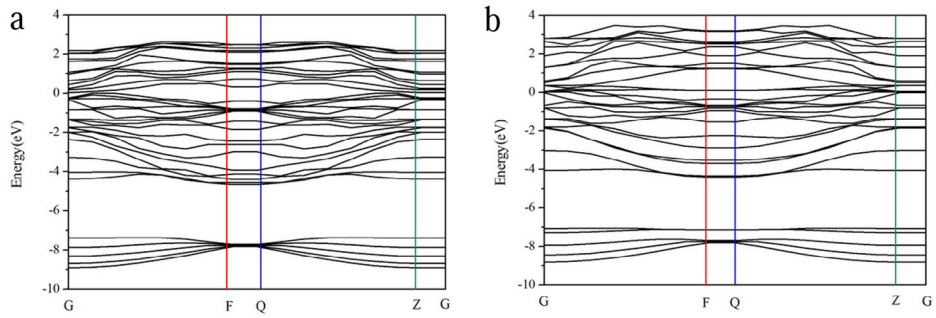

Fig. 3. Band structures of (a) Mg-termination surfaces, (b) Sn-termination surfaces.

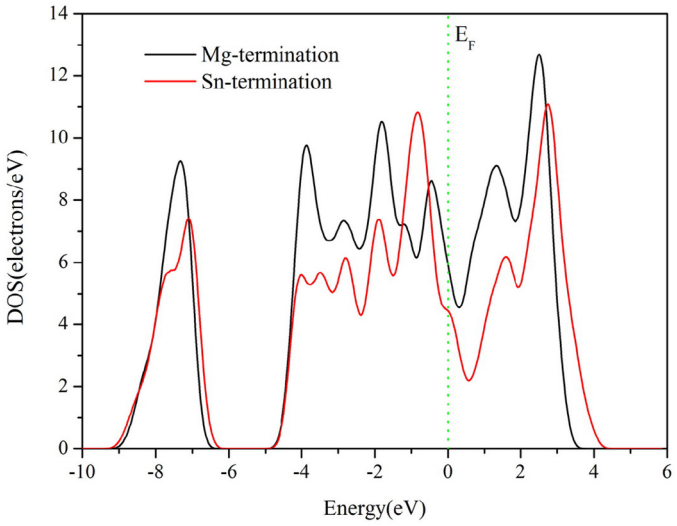

Fig. 4. Density of states (DOS) of Mg-termination surfaces and Sn-termination surfaces. The dash green line refers to Fermi level.

atomic interaction between the first Mg layer and the first Sn layer than that between other layers. Additionally, it is worth noting that the *s* and *p* states of Mg atoms and the *p* states of Sn atoms appear peaks simultaneously at the range from −5 eV to 0 eV, which implies that there is an electron overlap of the *s* and *p* states of Mg atoms and the *p* states of Sn atoms. The electron overlap indicates that there is hybridization between the *s* and *p* states of Mg atoms and the *p* states of Sn atoms.

The layer-atom PDOS of Sn-termination surfaces is shown in Fig. 6. As we can see from Fig. 6, the low energy area is mainly made up of Sn atoms below Fermi level, while the Mg atoms contribute to the high energy area above the Fermi level. It is obviously found that the *p* states of the first Sn layer from −4 eV to 0 eV are sharper and narrower than those of the second and third Sn layers. Furthermore, the *p* states of the first Sn layer and the *p* states of the first Mg layer appear sharp peaks simultaneously from −2 eV to 0 eV, indicating strong hybridization between *p* states of the first Sn layer and *p* states of the first Mg layer. Additionally, the PDOS of Sn-termination surfaces shifts to high energy area, which demonstrates that Mg-termination surfaces are more stable than Sn-termination surfaces. It should be pointed out that the charge density is neglected due to its little value for revealing surface electronic structures. In this work, the surface relaxation is a fully free process without surface reconstruction, which means no charge transfer occurs. Therefore, it is unnecessary to present and analyze the charge density.

4. Conclusions

In summary, surface relaxation, surface stability and electronic properties of Mg_2Sn (100) surfaces were investigated from first-principles method on the basis of DFT. Mg-termination and Sn-termination slab models were employed to establish the the Mg_2Sn (100) surfaces. The main conclusions were generalized as follows:

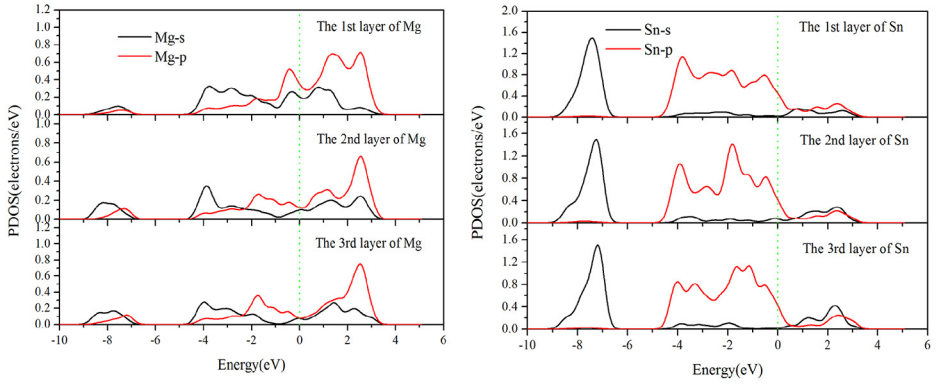

Fig. 5. Layer-atom partial density of states (PDOS) of Mg-termination surfaces.

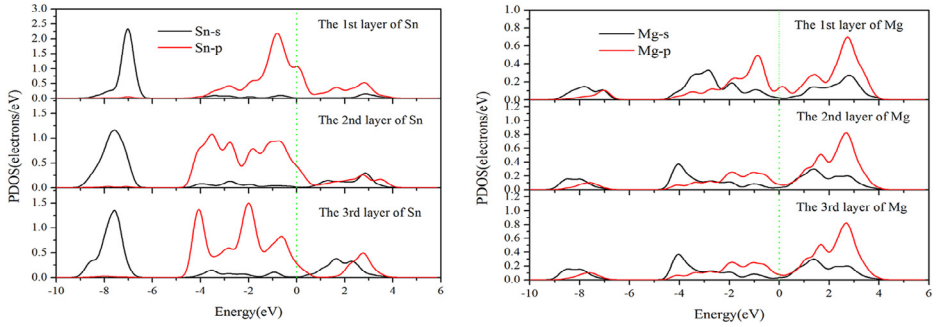

Fig. 6. Layer-atom partial density of states (PDOS) of Sn-termination surfaces.

(1) The surface optimization indicates that both the eleven-layers for Mg-termination surfaces and the nine-layers for Sn-termination surfaces are all converged very well.
(2) The effects of relaxation are mainly localized within the three outermost atomic layers for Mg-termination surfaces as well as Sn-termination surfaces. The changes between atomic layer distances of Sn-termination surfaces are slightly larger than those of Mg-termination surfaces.
(3) Mg-termination surfaces are more stable than Sn-termination surfaces since the surface energy of Mg-termination surfaces is lower than that of Sn-termination surfaces over nearly entire area of Mg chemical potentials $\left(\mu_{Mg}^{slab} - \mu_{Mg}^{bulk}\right)$.
(4) There are no band gaps in Mg-termination and Sn-termination surfaces. Both Mg-termination and Sn-termination surfaces are metallic characterization. It is found that covalent bonding exists in both Mg-termination and Sn-termination surfaces by analyzing the PDOS, and the covalent bonding in Sn-termination surfaces is stronger than that in Mg-termination surfaces.

Acknowledgments

This work was supported by the National Natural Science Foundation of China (Nos. 51464034 and 51301107).

References

[1] A.A. Nayeb-Hashemi, J.B. Clark, Phase Diagrams of Binary Magnesium Alloys, ASM International, Materials Park, OH, 1988.
[2] L. Zhang, Z.Y. Cao, Y.B. Liu, G.H. Su, L.R. Cheng, Mater. Sci. Eng. A 508 (2009) 129–133.
[3] C.L. Mendis, C.J. Bettles, M.A. Gibson, C.R. Hutchinson, Mater. Sci. Eng. A 435 (2006) 163–171.
[4] T.T. Sasaki, J.D. Ju, K. Hono, K.S. Shin, Scr. Mater. 61 (2009) 80–83.
[5] M.A. Gibson, X.Y. Fang, C.J. Bettles, C.R. Hutchinson, Scr. Mater. 63 (2010) 899–902.
[6] S.S. Park, B.S. You, Scr. Mater. 65 (2011) 202–205.
[7] T.T. Sasaki, K. Yamamoto, T. Honma, S. Kamado, K. Hono, Scr. Mater. 59 (2008) 1111–1114.
[8] H. Le-Quoc, A. Lacoste, E.K. Hlil, A. Bès, T.T. Vinh, D. Fruchart, et al., J. Alloy. Compd. 509 (2011) 9906–9911.
[9] R.G. Schwartz, H. Shanks, B.C. Gerstein, J. Solid State Chem. 3 (1971) 533–540.
[10] Y. Liu, W.C. Hu, D.J. Li, X.Q. Zeng, C.S. Xu, X.J. Yang, Intermetallics 31 (2012) 257–263.
[11] Y. Liu, W.C. Hu, D.J. Li, X.Q. Zeng, C.S. Xu, Appl. Phys. A-Mater. 115 (2014) 323–331.
[12] Y. Liu, W.C. Hu, D.J. Li, K. Li, H.L. Jin, Y.X. Xu, et al., Mater. Sci. 97 (2015) 75–85.
[13] B.H. Kim, J.J. Jeon, K.C. Park, B.G. Park, Y.H. Park, I.M. Park, Int. J. Cast. Metal. Res. 21 (1–4) (2008) 186–192.
[14] D. Luo, H.Y. Wang, Z.T. Ou-Yang, L. Chen, J.G. Wang, Q.C. Jiang, Mater. Lett. 94 (2013) 51–54.
[15] H.Y. Wang, X.L. Nan, N. Zhang, C. Wang, J.G. Wang, Q.C. Jiang, Mater. Chem. Phys. 132 (2012) 248–252.
[16] T.T. Sasaki, K. Oh-Ishi, T. Ohkubo, K. Hono, Scr. Mater. 55 (2006) 251–254.
[17] T.T. Sasaki, K. Oh-Ishi, T. Ohkubo, K. Hono, Mater. Sci. Eng. A 530 (2011) 1–8.
[18] Y.A. Chen, L. Jin, Y. Song, H. Liu, R. Ye, Mater. Sci. Eng. A 612 (2014) 96–101.
[19] X. Liu, D. Shan, Y. Song, R. Chen, E. Han, Electrochim. Acta 56 (2011) 2582–2590.
[20] G. Urretavizcaya, G.O. Meyer, J. Alloy. Compd. 339 (2002) 211–215.
[21] W.C. Hu, Y. Liu, D.J. Li, X.Q. Zeng, C.S. Xu, Physica B 427 (2013) 85–90.
[22] Y. Liu, W.C. Hu, D.J. Li, X.Q. Zeng, C.S. Xu, X.J. Yang, Physica B 432 (2014) 33–39.
[23] W.C. Hu, Y. Liu, D.J. Li, X.Q. Zeng, C.S. Xu, Mater. Sci. 83 (2014) 27–34.
[24] W.C. Hu, Y. Liu, D.J. Li, K. Li, H.L. Jin, Y.X. Xu, et al., Philos. Mag. 94 (2014) 3945–3959.
[25] F. Yu, J.X. Sun, T.H. Chen, Physica B 406 (2011) 1789–1794.
[26] R. Viennois, P. Jund, C. Colinet, J.C. Tédenac, J. Solid State Chem. 193 (2012) 133–136.
[27] S. Ganeshan, S.L. Shang, Y. Wang, Z.K. Liu, J. Alloy. Compd. 498 (2010) 191–198.
[28] D. Zhou, J. Liu, S. Xu, P. Peng, Comp. Mater. Sci. 51 (2012) 409–414.
[29] T.W. Fan, J.L. Ke, L. Fu, B.Y. Tang, L.M. Peng, W.J. Ding, J. Magnes. Alloy. 1 (2013) 163–168.
[30] Y. Liu, W.C. Hu, D.J. Li, X.Q. Zeng, C.S. Xu, Phys. Scr. 88 (2013) 45302–45310.
[31] P. Hohenberg, W. Kohn, Phys. Rev. B 136 (1964) 864–871.
[32] M.D. Segall, P.J. Lindan, M.A. Probert, C.J. Pickard, P.J. Hasnip, S.J. Clark, et al., J. Phys. Condens. Matter 14 (2002) 2717–2744.
[33] D. Vanderbilt, Phys. Rev. B 41 (1990) 7892–7895.
[34] K. Laasonen, A. Pasqurello, R. Car, C. Lee, D. Vanderbilt, Phys. Rev. B 47 (1993) 10142–10153.
[35] J.P. Perdew, K. Burke, M. Ernzerhof, Phys. Rev. Lett. 77 (1996) 3865–3868.
[36] T.H. Fischer, J. Almlof, J. Phys. Chem. 96 (1992) 9768–9774.
[37] B.G. Pfrommer, M. Côté, S.G. Louie, M.L. Cohen, J. Comput. Phys. 131 (1997) 233–240.
[38] S. Ganeshan, S.L. Shang, H. Zhang, Y. Wang, M. Mantina, Z.K. Liu, Intermetallics 17 (2009) 313–318.
[39] L.C. Davis, W.B. Whitten, G.C. Danielson, J. Phys. Chem. Solids 28 (1967) 439–447.
[40] O. Benhelal, A. Chahed, S. Laksari, B. Abbar, B. Bouhafs, H. Aourag, Phys. Status Solidi B 242 (2005) 2022–2032.
[41] Q.J. Liu, Z.T. Liu, J.C. Chen, L.P. Feng, H. Tian, W. Zeng, Appl. Surf. Sci. 258 (2012) 3455–3461.
[42] K. Rapcewicz, B. Chen, B. Yakobson, J. Bernholc, Phys. Rev. B 57 (1998) 7281–7291.
[43] I. Batyrev, A. Alavi, M.W. Finnis, Faraday Discuss. 114 (1999) 33–43.
[44] H. Zhang, S. Shang, J.E. Saal, A. Saengdeejing, Y. Wang, L.Q. Chen, et al., Intermetallics 17 (2009) 878–885.
[45] W. Liu, C. Wang, J. Cui, Z.Y. Man, Solid State Commun. 149 (2009) 1871–1876.
[46] I.H. Jung, D.H. Kang, W.J. Park, N.J. Kim, S. Ahn, Calphad 31 (2007) 192–200.
[47] F.G. Meng, J. Wang, L.B. Liu, Z.P. Jin, J. Alloy. Compd. 508 (2010) 570–581.